Calibrating the γ-Re_θ Transition Model for Commercial CFD

Paul Malan[1]
CD-adapco, Lebanon, NH 03766

Keerati Suluksna[2] and Ekachai Juntasaro[3]
Suranaree University of Technology, Nakhon Ratchasima 30000, Thailand

The correlation-based γ-Re_θ transition model is designed for implementation in modern unstructured, parallel CFD codes. So far, this model has been published in incomplete form, with two key correlations, $Re_{\theta c}$ and F_{length}, being kept proprietary. This paper describes the implementation of the γ-Re_θ transition model in a commercial CFD code, including a description of the process of calibrating the key correlations using published data. Results are presented for flat plate boundary layers, with and without pressure gradient, and for airfoil and turbomachinery flows. A 3D multi-element airfoil simulation is presented as an example of an industrial test case.

Nomenclature

k	=	turbulent kinetic energy
C	=	chord length
C_f	=	skin friction coefficient
C_p	=	pressure coefficient
F_{length}	=	function to control transition length
F_{onset}	=	function to control transition onset location
L	=	flat plate length
Re_θ	=	momentum thickness Reynolds number
$Re_{\theta c}$	=	momentum thickness Reynolds number where the intermittency starts to increase
$Re_{\theta t}$	=	momentum thickness Reynolds number where the skin friction starts to increase
$\tilde{Re}_{\theta t}$	=	transported variable for $Re_{\theta t}$
S	=	streamwise distance
Tu	=	turbulence intensity expressed as a percentage
U	=	velocity magnitude
u^*	=	friction velocity
x	=	distance along flat plate
y	=	wall-normal distance
y^+	=	non-dimensional wall-normal distance, $\rho y u^*/\nu$
γ	=	intermittency
δ_{99}	=	boundary layer thickness
μ	=	dynamic viscosity
μ_t	=	turbulent viscosity
ρ	=	density
ω	=	specific dissipation rate

[1] Senior Research Engineer, CD-adapco, New Hampshire Office, 21 Lafayette Str., Suite 230, Lebanon, NH 03766. Senior Member.
[2] Lecturer, School of Mechanical Engineering, Institute of Engineering, Suranaree University of Technology, Nakhon Ratchasima 30000, Thailand.
[3] Associate Professor, School of Mechanical Engineering, Institute of Engineering, Suranaree University of Technology, Nakhon Ratchasima 30000, Thailand.

I. Introduction

TRANSITIONAL boundary layer flows are important in many CFD applications of engineering interest, such as airfoils, wind turbines, boat hulls and turbomachinery blade rows. Unfortunately, modern unstructured, parallel CFD codes do not lend themselves to traditional correlation-based methods for transition prediction. These methods are based on non-local variables such as momentum thickness or boundary layer edge location, which can be expensive, impractical, or even practically impossible to evaluate. The γ-Re_θ transition model, introduced by Menter *et al.* [1] in 2004, presented for the first time a correlation-based approach to transition modeling that was designed specifically for modern CFD codes. Unfortunately, the model has not gained wide acceptance in the CFD community because two critical correlations were deemed proprietary and have remained unpublished by the original authors, even as their model has been refined in subsequent publications.[2-5] Arguably, the model is a useful framework into which prospective users might insert their own correlations based on their own data and/or data from the public domain. Few CFD practitioners, however, have the resources or expertise to develop such correlations.

Recently, efforts by independent research groups to synthesize the two missing correlations have started to bear fruit.[6-7] A systematic effort at the Suranaree University of Technology, Thailand,[7] has resulted in proposed forms for these correlations that are believed to capture the essential behavior of the γ-Re_θ transition model as documented by Menter *et al.*, [1-5] along with a viable methodology for "tuning" the correlations for a specific CFD code. Such tuning is thought to be necessitated by small implementation differences that might exist between different codes, such as the discretization approach or the adoption of alternative variants of the base turbulence model. These small differences can affect the ability of the correlations, calibrated in one code, to function accurately in a different code.

In this paper, the implementation of the γ-Re_θ transition model in a modern commercial CFD code, STAR-CCM+[8] is discussed and the forms of the missing correlations are described and analyzed. The calibration approach using zero-pressure gradient, flat plate data is presented first, followed by tests of the model against non-zero pressure gradient test cases for which data are freely available. Finally, an example of an industrial application of the model to a 3D multi-element airfoil is presented.

II. Model Implementation

STAR-CCM+ has been developed with a client-server architecture using object-oriented methods in C++ and Java. It uses a cell centered, finite volume discretization approach applied to cells of arbitrary polyhedral shapes. Two flow solver algorithms are available: a segregated approach using Rhie-Chow interpolation (see, for example, Demirdzic and Muzaferija[9]) and a coupled approach using the preconditioning of Weiss and Smith.[10] A wide range of turbulence models is provided, including the SST k-ω model of Menter[11-12] which is a prerequisite for the γ-Re_θ transition model. STAR-CCM+ embodies the state-of-the-art of modern software development methods, which allows rapid model implementation. Nevertheless, the approach described herein for calibrating the γ-Re_θ transition model could be applied to any CFD code.

The formulation of Menter's SST k-ω turbulence model[11-12] and the γ-Re_θ transition model[1-5] in STAR-CCM+ is given in the appendix. The turbulence model is a reasonably standard implementation with several exceptions. First, the wall boundary condition for ω is specified within the wall cell, rather than at the boundary as suggested by Menter.[11] This allows compatibility with wall functions to be maintained, although only low-Reynolds number wall treatments are used in the present study. Second, in accordance with later recommendations,[12] the strain rate tensor modulus is used in the production term rather than the vorticity as in the original model formulation.[11] Third, the realizability constraint of Durbin[13] is used as opposed to the less restrictive bound on the production favored by the originator of the SST k-ω turbulence model.[12] Experience with validating and applying Durbin's constraint to industrial simulations in STAR-CCM+ has thus far shown no significant adverse effects.

The transport equations for both the SST k-ω turbulence model and the γ-Re_θ transition model are implemented in STAR-CCM+ with a second-order upwind scheme. This advection scheme was also used for the momentum equation, and where applicable, the energy equation.

A feature of STAR-CCM+ that lends itself to the implementation of the γ-Re_θ transition model as a customizable framework is User Field Functions. These are single-line, interpreted C-syntax statements that allow the manipulation of fields (stored variables) and other User Field Functions. These may be predefined in the model, but can also be created and easily modified by the user.

The γ-Re_θ transition model requires that the transition onset momentum thickness Reynolds number, $Re_{\theta t}$, be specified in the free stream. Since $Re_{\theta t}$ is a non-local quantity, two noteworthy complications arise. First, one must define what (or where) the free stream is. Second, the source term evaluation of transport equation for $\tilde{R}e_{\theta t}$ requires that cells inside the boundary layer reference the value of $Re_{\theta t}$ in the free stream. In the STAR-CCM+ implementation, the first issue has been addressed somewhat vaguely by allowing the user to specify the location of the free stream in terms of an iso-surface defined by User Field Function. A typical iso-value definition might be based on wall distance (used in most of the test cases reported herein) or the value of the vorticity vector magnitude. The second issue is addressed by using a KD tree algorithm to store the location of the mesh faces that most closely correspond to the free stream definition. The flow variables of interest are then interpolated from the cell values straddling the face. This introduces an unavoidable computational overhead when run in parallel, since the KD tree must be broadcast to each parallel node. Since the free-stream edge can potentially vary with each iteration, the tree cannot be stored, so the tree is updated only every *n* iterations as a cost saving measure.

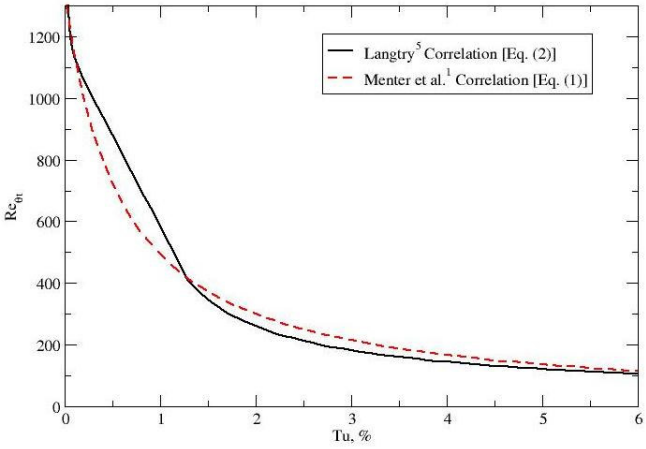

Figure 1. Comparison of $Re_{\theta t}$ correlations.

III. Model Calibration Using Zero-Pressure Gradient Flat Plate Data

As described in the appendix, three correlations are required to close the γ-Re_θ transition model: $Re_{\theta t}$, $Re_{\theta c}$ and F_{length}. The first of these have been presented in two alternative forms[1,5] so one only has to make a choice between them. The other two correlations are derived from calibration against zero-pressure gradient flat plate data.

Reffering to Eqs. (19) and (24), it can be seen that for the case of zero pressure gradient, $\lambda = K = 0$, so that $F = F_{\lambda,K} = 1$. These two correlations are compared in Fig. 1 for zero pressure gradient. The curve of Eq. (19) is a better fit to the experimental data cited in Refs. 1 and 5. However, according to Langtry,[5] the rationale for changing this curve was "to improve the results" for $Tu < 1\%$. Both correlations were implemented in STAR-CCM+ for the purpose of evaluation, but as will be explained, Eq. (24) was finally adopted.

The parameters $Re_{\theta c}$ and F_{length} are both expressed as functions of $\tilde{R}e_{\theta t}$, the transported transition momentum thickness Reynolds number. Viable forms for $Re_{\theta c}$ and F_{onset} were obtained by physical intuition and numerical experiment as described by Suluksna *et al.*[7] In this process, it is hypothesized that $Re_{\theta c}$ is a low-order polynomial (preferably linear) function of $\tilde{R}e_{\theta t}$. The rationale for this hypothesis is as follows. In the free stream, $\tilde{R}e_{\theta t} = Re_{\theta t}$ by design. One can also assume that $Re_{\theta c} < Re_{\theta t}$, since $Re_{\theta c}$ is the momentum thickness Reynolds number at which intermittency first starts to grow, and $Re_{\theta t}$ is the momentum thickness Reynolds number where the skin friction starts to increase. Therefore, the form $Re_{\theta c} = a\tilde{R}e_{\theta t} + b$ seems like a reasonable starting point, where a is some number of order one but less than unity. Furthermore Langtry[5] suggests a lower bound of 20 on $Re_{\theta t}$, which will in turn bound $\tilde{R}e_{\theta t}$ and $Re_{\theta c}$. It is also clear from the model formulation that adjusting the coefficients in a manner that increases $Re_{\theta c}$ will result in an earlier transition onset. This can be seen from the model equations, in which increasing $Re_{\theta c}$ increases F_{onset}, the parameter governing where intermittency first starts to increase in the boundary layer.

Simulations based on the ERCOFTAC data[13] for cases T3A, T3B and T3AM were used to find the form of the F_{length} function.[7] By assuming a linear function for $Re_{\theta c}$ as suggested above, these numerical experiments showed that F_{length} is a small number for large values of $\tilde{R}e_{\theta t}$ (*i.e.*, low turbulence intensities) and *vice versa*. Furthermore, the solution is relatively insensitive to the exact value of F_{length} for small values $\tilde{R}e_{\theta t}$ (*i.e.*, high turbulence intensities). Since the ERCOFTAC data correspond to moderately low- to high- turbulence intensity bypass transition, the natural transition skin friction data of Schubauer and Klebanoff,[13] digitized from Langtry[5] and termed TSK herein, were added to the calibration data sets.

The calibration process started with an assumed value of the coefficients a and b for the $\mathrm{Re}_{\theta c}$ curve (say $a = 0.8$, $b = 0$) and an assumed constant value for F_{length}, say ($0.3 < F_{length} < 0.7$). The lower free-stream turbulence cases TSK and T3AM cases were then run, and the coefficients adjusted to get the best curve fit to the data. The T3A and T3B cases could then be run to update the coefficients in an iterative process. The approximate F_{length} curve shape for T3A and T3B was established by assuming that F_{length} is proportional to some representative wall value of $\tilde{\mathrm{Re}}_{\theta t}$, such as the value at the leading edge. This numerical tuning resulted in the following expressions:

$$\mathrm{Re}_{\theta c} = \min\left(0.625\tilde{\mathrm{Re}}_{\theta t} + 62, \tilde{\mathrm{Re}}_{\theta t}\right) \tag{1}$$

$$F_{length} = \min\left[0.01\exp\left(-0.022\tilde{\mathrm{Re}}_{\theta t} + 12\right) + 0.57, 300\right] \tag{2}$$

Eqs. (1) and (2) are shown graphically in Fig. 2. The grey area represents the range of F_{length} values which would be viable for high free-stream turbulence intensities. We chose the lower bound of the envelope since this appeared to improve solution convergence.

It should be mentioned that these calibrated correlations are valid only when used with the $\mathrm{Re}_{\theta t}$ correlation of Eq. (24). A similar calibration procedure was successfully carried out for Eq. (19), but was not pursued further since a quadratic polynomial form for $\mathrm{Re}_{\theta c}$ was required to reproduce the required correspondence to the experimental data. It seems plausible that this is the reason behind the modification of the $\mathrm{Re}_{\theta t}$ correlation as reported by Langtry.[5]

The computational mesh used for the calibration studies is shown schematically in Fig. 3. The domain extended from 0.15m upstream of the plate to 1.7m downstream. The domain height was 0.3m. A specified constant velocity inlet was used together with a specified constant static pressure at outlet. Slip walls were used on the top boundary and upstream of the plate. The inflow boundary conditions are reported in Table 1. Fluid density was taken to be 1.2 kg/m^3 and viscosity 1.8x10^{-5} PaS.

The mesh contained 100x135 quad cells, with a near-wall cell height of 10^{-5}m, ensuring

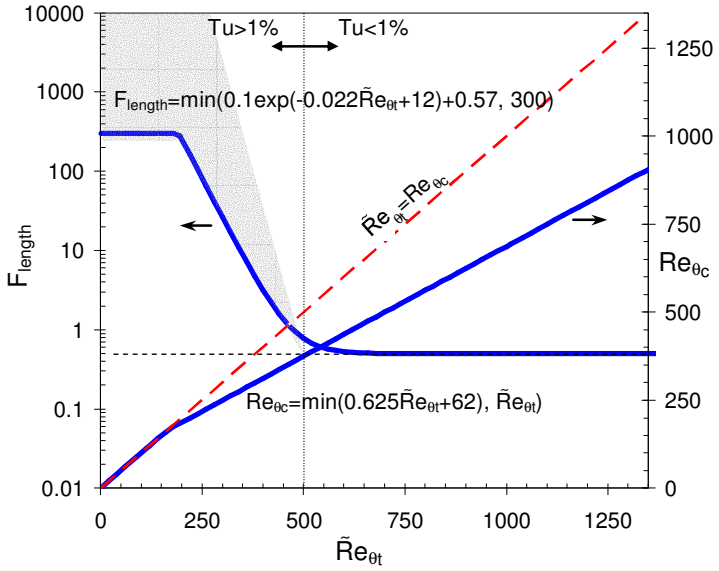

Figure 2. Calibrated correlations for $\mathrm{Re}_{\theta t}$ and F_{length}

Case	U_{in} (m/s)	k_{in} (J/kg)	ω_{in} (/s)
TSK	50.1	0.0827	5134
T3AM	19.8	0.0780	680.4
T3A	5.40	0.1386	712.2
T3B	9.40	0.8964	573.2

Table 1. Inflow boundary conditions for zero pressure gradient flat plate simulations.

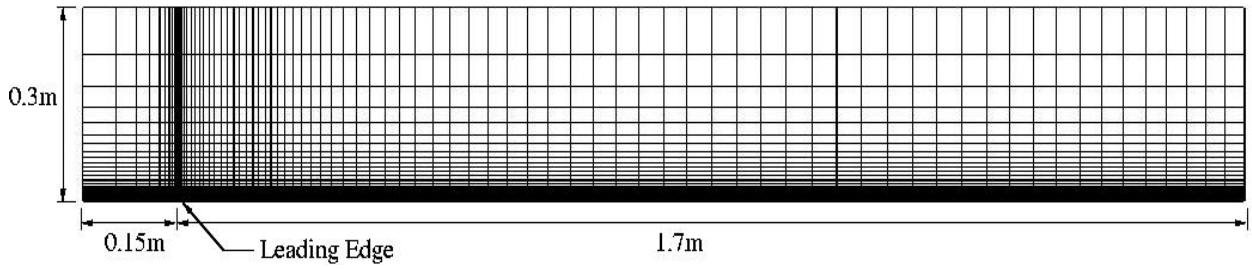

Figure 3. Mesh schematic for zero pressure gradient flat plate simulations.

that the wall-adjacent cell centroid height typically ranged between 0.2 and 0.5 viscous units. Since the model was calibrated using this mesh, particular attention was paid to mesh sensitivity. It was found that the T3AM and TSK cases were especially sensitive to the streamwise spacing near the end of the plate, and also to the domain height. Results obtained by doubling the mesh resolution in both coordinate directions confirmed that the mesh described herein produces a mesh-independent solution.

The skin friction coefficient results of the TSK, T3AM, T3A, and T3B simulations are shown in Fig. 4, with the free-stream turbulence intensity decay profiles in Fig. 5. For case TSK, the turbulence decay profiles are not readily available, so the inflow boundary conditions were chosen to match the leading edge values of turbulence intensity and viscosity ratio (R_T) quoted by Langtry.[5] It should be pointed out that these results are not evidence of the predictive capabilities of the γ-Re_θ transition model, since the model correlations were specifically adjusted to cause the model to properly match the data. Overall, the skin friction coefficient results are comparable to those presented by Langtry.[5]

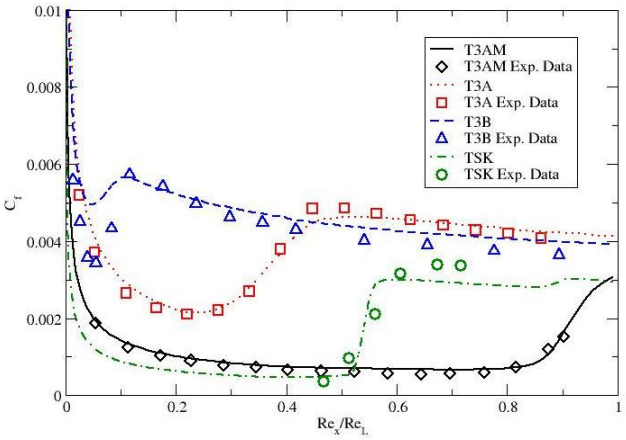

Figure 4. Skin friction coefficient results for zero pressure gradient flat plate simulations after model calibration.

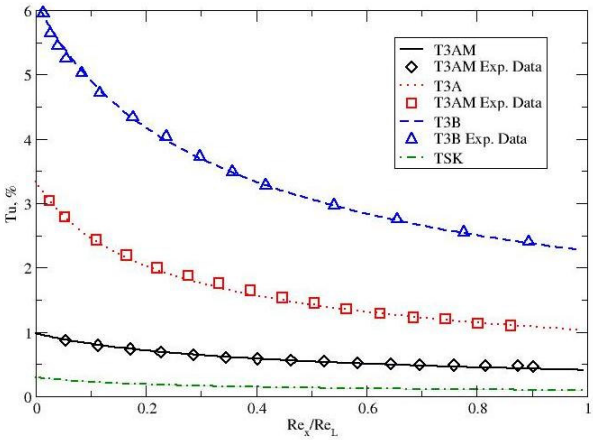

Figure 5. Freestream turbulence decay for zero pressure gradient flat plate simulations.

IV. Validation Against Non-Zero-Pressure Gradient Flat Plate Data

ERCOFTAC cases T3C1-5 test the combined effect of pressure gradient and free-stream turbulence decay on the transition prediction. They are considerably more difficult to set up since they require the prescription of a variable free-stream velocity, as well as a definition of the free-stream location. This was achieved by using continuity to estimate a suitable area variation in the duct, as shown in Fig. 6. A different shape was required for case T3C4 than the others. Polynomial expressions for the duct shapes are given by Suluksna *et al.*[7] The mesh size used was 60x146 cells, with a near-wall mesh spacing of 10^{-5}m. Mesh independence will be confirmed for the final paper.

Since the data indicate elevated levels of turbulence intensity at $y=\delta_{99}$, the free stream edge location was taken to be $y=2\delta_{99}$ for the purposes of these simulations. Reference turbulence intensities and streamwise velocities at $y=2\delta_{99}$ were linearly interpolated from the data at each measurement station. A polynomial curve fit to the data was used to specify the free stream location to fulfill the requirement of the γ-Re_θ model.

Material properties were the same as for the zero-pressure gradient cases. Slip walls were used on the top boundary and upstream of the plate. The inflow boundary conditions are reported in Table 2. To facilitate a better match to the turbulence intensity profiles, the turbulence decay was deactivated upstream of the plate, so that the inlet values are, in effect, leading edge values. These conditions were specified in terms of turbulence intensity and viscosity ratio, $Tu = \sqrt{2/3k}\,/U$ and $\mu_t/\mu = \rho k/(\omega\mu)$.

Case	U_{in} (m/s)	*Tu (%)*	μ_t/μ
T3C1	6.1	7.78	44
T3C2	5.25	3.1	9
T3C3	3.95	3.1	6
T3C4	1.28	2.8	2
T3C5	8.8	4.5	11

Table 2. Inflow boundary conditions for non-zero-pressure gradient flat plate simulations.

Figs. 7 and 8 show the correspondence of the free-

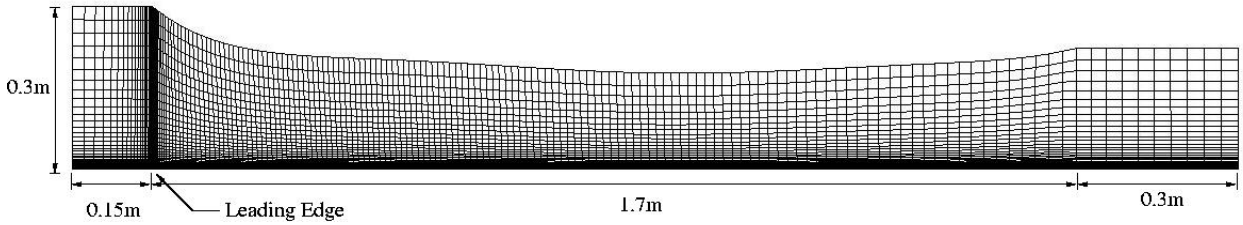

Figure 6. Mesh schematic for non-zero-pressure gradient flat plate simulations.

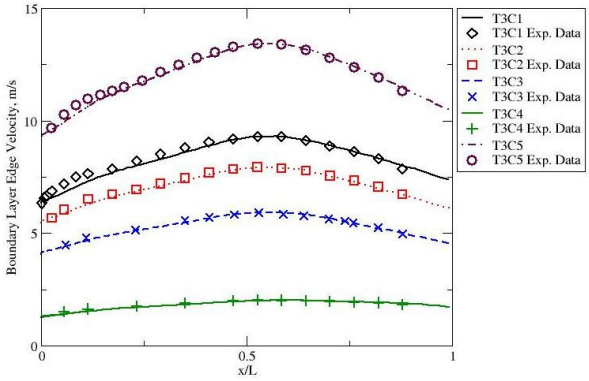

Figure 7. Free-stream velocity profiles for non-zero-pressure gradient cases.

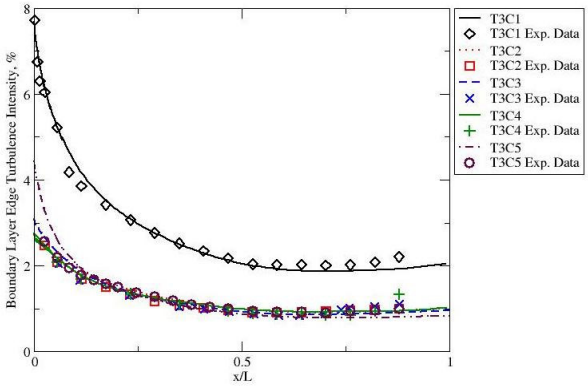

Figure 8. Free-stream turbulence decay for non-zero-pressure gradient cases.

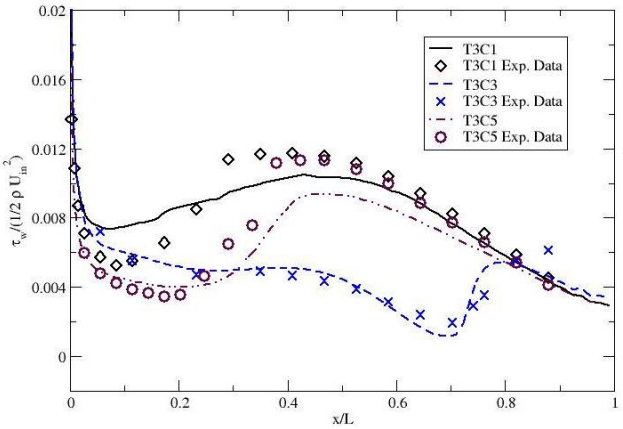

Figure 9. Skin friction coefficient results for cases T3C1, T3C3 and T3C5.

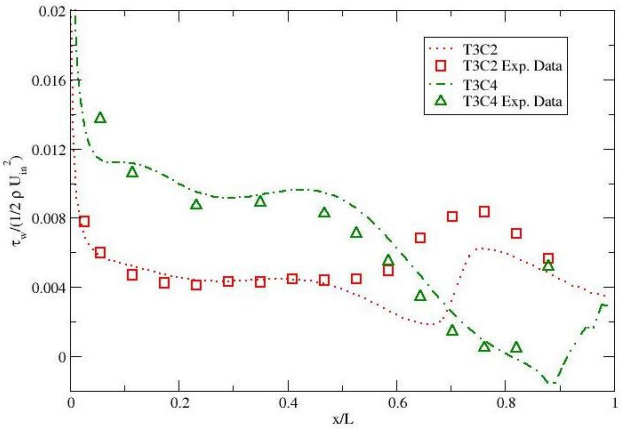

Figure 10. Skin friction coefficient results for cases T3C2 and T3C4.

stream velocity and turbulence intensity to the data. Some discrepancies occur near the leading edge of the plate ($x/L < 0.2$). These reflect the compromises that were required to reasonably match the free stream conditions over the bulk of the plate.

Skin friction coefficient results for cases T3C1, T3C3 and T3C5 are shown in Fig. 9 and for T3C2 and T3C4 in Fig 10. For simplicity, the wall shear stress is non-dimensionalized by the inflow velocity rather than the free stream flow velocity (the experimental data as well as the simulation results).

In general, the results are similar to those reported by Langtry,[5] although by using a boundary layer code for cases T3C2, T3C3 and T3C5, Langtry[5] was able to exercise more control over the free-stream conditions. Case T3C1 (not reported by Langtry[5]) experiences an early onset of transition due to the high free-stream turbulence intensities. Similar to the T3B case, skin friction coefficient is somewhat high in the transition region. Case T3C2 represents transition near the suction peak, and the onset is predicted too far downstream, consistent with the results of Langtry[5]. The results of case T3C3, where separation occurs in an adverse pressure gradient are excellent. Case

T3C4 represents transition due to the presence of a laminar separation bubble, which was properly captured, although a little far downstream. Finally, the higher Reynolds number case T3C5 shows the behavior of the model in a favorable pressure gradient. Consistent with the results of Langtry[5], the onset of transition is slightly too far downstream.

One very important outcome of these non-zero-pressure gradient flat plate cases was the conclusion that the function F in Eq. (24) needs to be set to unity for best results. In other words, *the effects of stream-wise pressure gradient were explicitly omitted in the evaluation of* $\mathrm{Re}_{\theta t}$. Suluksna *et al.*[7] justify this omission with the explanation that, by expressing $\mathrm{Re}_{\theta t}$ as a function of Tu, pressure gradient effects are implicitly accounted for because of the effect of the pressure gradient on the local turbulence in the boundary layer. Simply put, adverse pressure gradients tend to promote turbulence whereas favorable pressure gradients suppress it. This assertion must be considered in the light of the fact that the original correlation of Eqs. (19)-(23) was based on the *leading edge* values of Tu, not local values.

V. Two-Dimensional Test Cases

Three 2D test cases are presented in this section: the Aerospatiale-A airfoil[16], the Zierke and Deutsch compressor cascade[17] and the VKI BRITE large scale turbine cascade measured at the University of Genoa. [18] Each of these cases have been considered by Langtry.[5]

Two sets of experimental data are available for the Aerospatiale-A airfoil, the F1 wind tunnel data at a 13.1° angle of attack at a Reynolds number of $2.07\text{x}10^6$, and the F2 wind tunnel data at 13.3° angle of attack and at a Reynolds number of $2.1\text{x}10^6$. The former condition was simulated herein, although F2 data for the skin friction and force coefficients are used as a basis of comparison. The C-topology computational mesh of 200x800 cells is shown in Fig. 11. The near-wall mesh spacing is 10^{-5} chord lengths, resulting in a peak value of y^+ ranging from approximately 0.25 on the pressure surface to a peak of 0.7 immediately downstream of transition on the suction surface. This mesh is fine enough to yield a mesh-independent result. The domain extends from 8 chord lengths upstream to 20 chord lengths downstream. Since the inflow boundary is non-planar, the inflow values of k and ω were specified with the appropriate analytical decay laws to obtain $Tu = 0.2\%$ and $\mu/\mu_t = 10$ at the leading edge plane. The free-stream edge definition for the γ-Re_θ model was arbitrarily defined as 0.05 chord lengths from the airfoil surface. The simulation results for pressure coefficient are compared to the F2 experimental data in Fig. 12, and the suction surface skin friction coefficient is compared to both the F1 and F2 data in Fig 13. The most significant deviation in the pressure coefficient distribution occurs at the trailing edge. This might be due to the fact that a sharp trailing edge was modeled. Transition on the suction surface is triggered by a laminar separation bubble at about 12% of chord. Turbulent separation occurs at about 96% chord, somewhat later than the experiment. The predicted lift and drag coefficients are 1.445 and 0.0169, which compare reasonably well with the F1 reported coefficients of 1.562 and 0.0208, respectively.

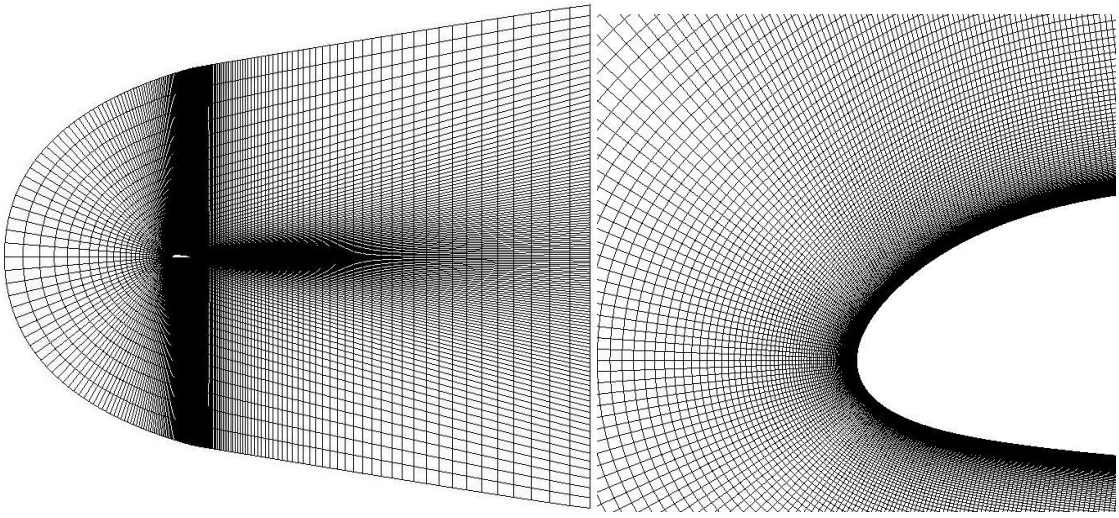

Figure 11. Mesh used for the Aerospatiale-A airfoil.

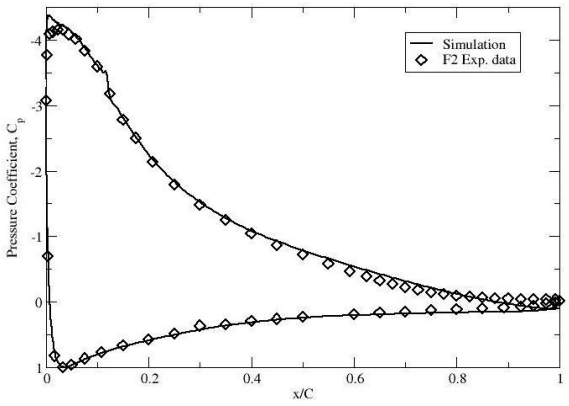

Figure 12. Pressure coefficient results for the Aerospatiale-A airfoil.

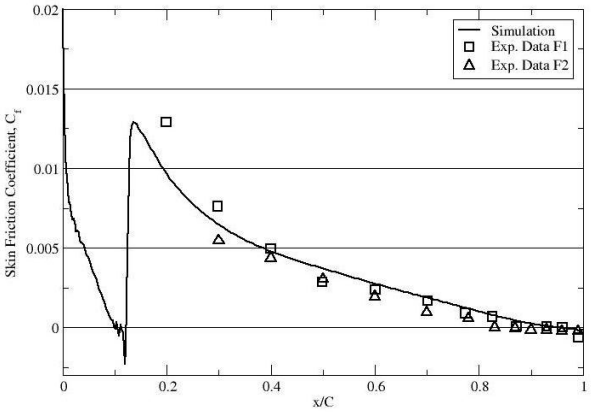

Figure 13. Skin friction coefficient on the suction surface for Aerospatiale-A airfoil.

The highly loaded compressor cascade case of Zierke and Deutsch[17] was simulated for the case of leading edge incidence angle of -1.5°. The computational mesh, consisting of 89,752 cells is shown in Fig 14. The wall-adjacent cell centroid height is 4×10^{-6}m, resulting in typical values of y^+ ranging from 0.1 to 0.6. The inflow was specified a distance of 0.3 axial chord lengths upstream. The inflow turbulence boundary conditions were $Tu = 0.2\%$ and $\mu/\mu_t = 2$. The free-stream edge definition for the γ-Re_θ model was arbitrarily defined as 5mm (approximately 2.3% of the axial chord length) from the blade surface.

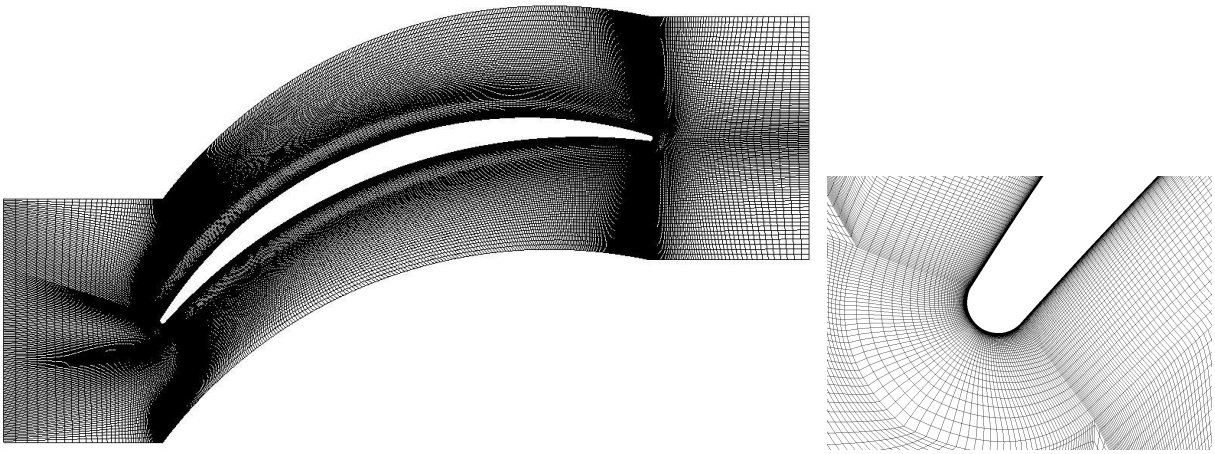

Figure 14. Mesh used for Zierke and Deutsch compressor cascade.

The pressure coefficient distribution is shown in Fig. 15 and the skin friction coefficient in Fig. 16. The various experimental data for skin friction represent the different methods used to derive this quantity from the measured velocity profiles. As reported by Langtry,[5] transition occurs immediately on the suction surface, triggered by a small laminar separation bubble at the leading edge. Transition is also triggered by laminar separation on the suction surface, but closer to mid-chord. The transition location in the present simulation is slightly further upstream than shown by the experimental data.

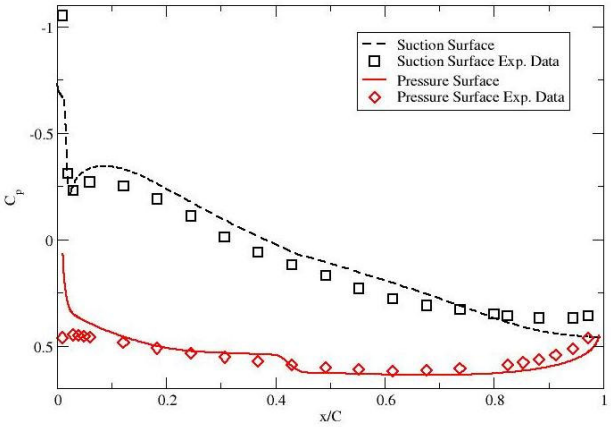

Figure 15. Pressure coefficient results for the Zierke and Deutsch compressor cascade.

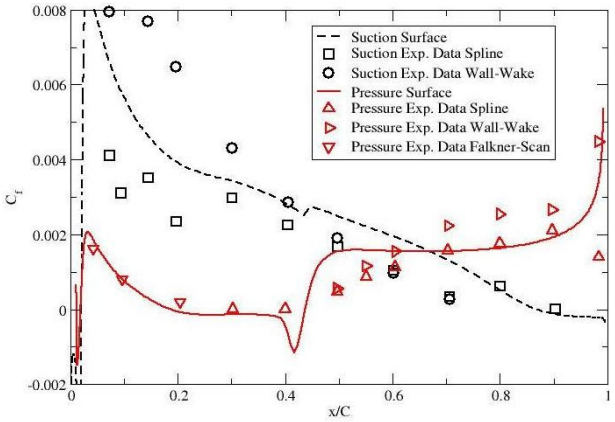

Figure 16. Skin coefficient results for the Zierke and Deutsch compressor cascade.

The computational mesh for the Genoa turbine cascade is shown in Fig. 17. An O-type mesh is used to surround the blade and the total cell count is 79,020. The near-wall cell centroid height was nominally $2\text{x}10^{-6}$m, although the mesh smoothing algorithm resulted in some scatter about this value. This mesh spacing resulted in a maximum y^+ value of approximately 0.65 on the suction surface.

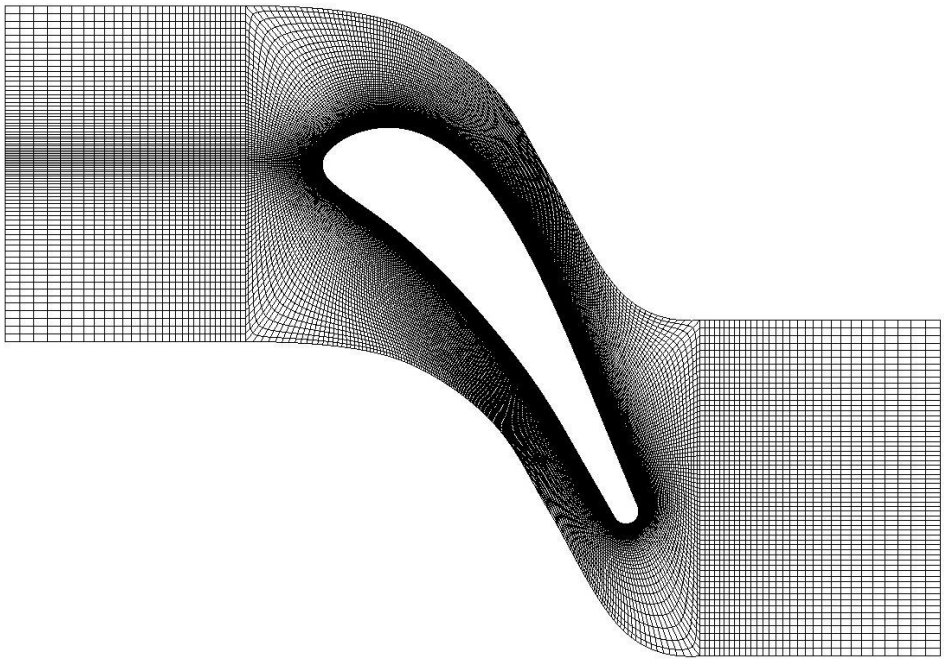

Figure 17. Mesh used for the Genoa turbine cascade.

The relative inlet total pressure is given as 3060 Pa, and, to match the required outlet isentropic Mach number, an outlet relative static pressure of -1041.97 was specified. The inflow turbulence boundary conditions were Tu = 4% and μ/μ_t = 80. These large values were required to match the experimental data in the free stream. The correspondence is shown in Fig. 18 for specific probe points corresponding to the outside edge of the boundary layer traverse planes. These turbulence conditions were considerably larger than the values used by Langtry,[5] who chose respective values of 1.5% and 1.5. The free-stream edge definition for the γ-Re_θ model was arbitrarily defined as 5mm (approximately 1.7% of the blade chord length) from the blade surface.

The isentropic velocity distribution is shown in Fig. 18 and the suction surface skin friction velocity, normalized by free-stream velocity, is shown in Fig. 19. The pressure surface skin friction is not plotted since the boundary layer remains laminar on that surface. Transition occurs somewhat further upstream on the suction surface than in

the experiment. The results shown by Langtry[5] also reflect an early transition, but not to the same extent. We attribute the slight discrepancy between our results and Langtry's to the choice of inflow turbulence conditions. Indeed, experimenting with the inflow turbulence showed that reducing the inflow turbulence intensity will delay transition, as might be expected.

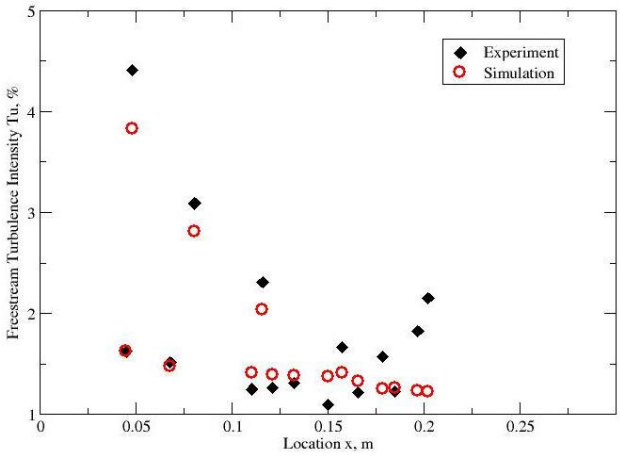

Figure 18. Free-stream turbulence intensity at boundary layer edge probe locations for the Genoa turbine cascade.

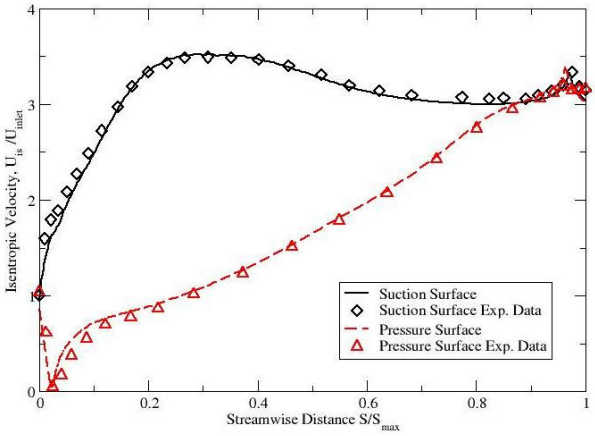

Figure 19. Isentropic velocity distribution for Genoa turbine cascade.

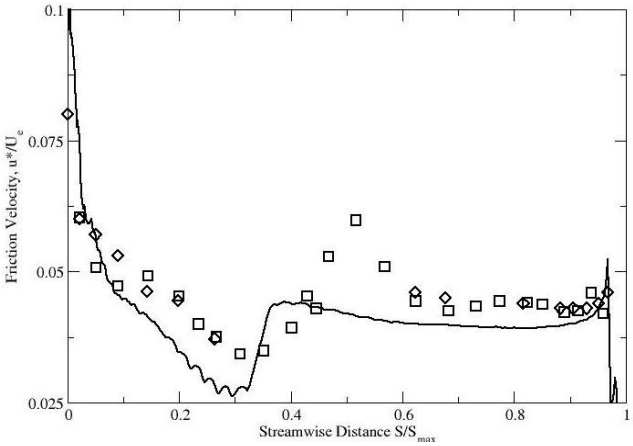

Figure 20. Normalized friction velocity on the Genoa turbine suction surface.

VI. Three-Dimensional Multi-Element Airfoil

The objective of the 3D multi-element airfoil simulation was to evaluate the performance of the γ-Re_θ transition model on a typical industrial application for which it was known *a priori* that transition prediction was important. The case selected was a Formula One car rear wing configuration. Wind tunnel flow visualization showed that a laminar separation occurred on the suction surface of the upper airfoil flap element, in addition to the turbulent separation further downstream. Flow simulations without a transition model can, therefore, not be relied on to accurately predict the force coefficients. The geometry and symmetry plane mesh is shown in Fig. 21, with a close-up of the surface mesh detail in Fig 22. The mesh comprised 12.8 million cells, and was created within STAR-CCM+ using the trimmed mesh approach. This approach uses a Cartesian mesh with hanging node refinement in the far field and achieves adequate

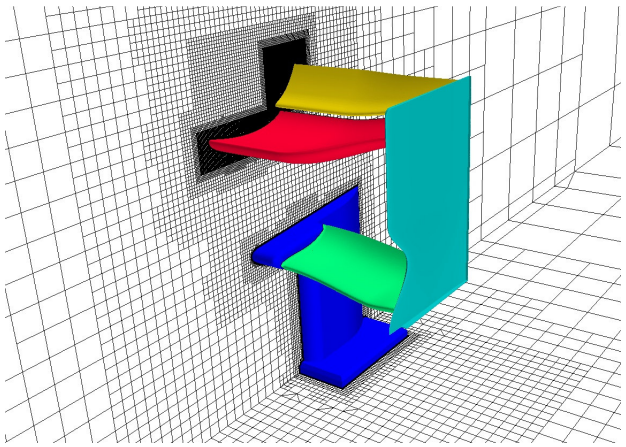

Figure 21 Multi-element airfoil geometry and symmetry plane mesh.

boundary layer resolution by extruding a prism mesh layer in a void created in the vicinity of the surfaces. The axial chord of the upper two-element airfoil is 0.334m at the symmetry plane. The Reynolds number based on this chord was 1.1×10^6. The wind tunnel inlet was placed approximately 9m upstream of the upper airfoil leading edge. Slip walls were used on all wind tunnel boundaries to avoid the need to resolve the boundary layers. The specified inflow turbulence boundary conditions were Tu = 2% and μ/μ_t = 100, resulting in a free-stream turbulence intensity at the airfoil leading edge of 0.45%. The free-stream edge definition for the γ-Re_θ model was arbitrarily defined as 3mm (approximately 1% of the axial chord) from the airfoil surface.

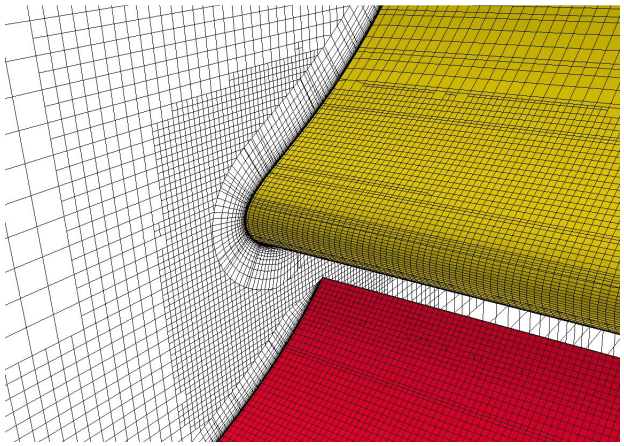

Figure 22. Mesh detail on airfoil surface and symmetry plan.

In industrial situations, mesh resolution is often driven by available computational resources, rather than the proper approach of demonstrating mesh independence. The current mesh is a representative example of the degree of resolution that a sophisticated industrial CFD practitioners might use. Nevertheless, a 25 million cell version will be run for the final paper to investigate the effects of further mesh refinement.

Fig. 23 shows the wind tunnel oil streak flow visualization on the suction surface of the flap. A similar view of streakline visualization from the STARCCM+ simulation is shown in Fig. 24. It is clear that the major features of laminar separation, transition to turbulence, and turbulent separation have been captured in the simulation, although the spanwise distribution of the turbulent separation location is not perfectly replicated. Still, this example shows that the γ-Re_θ transition model can produce realistic flow features on a realistic 3D geometry and a reasonably representative mesh. Pressure coefficient data will also be shown in the final paper.

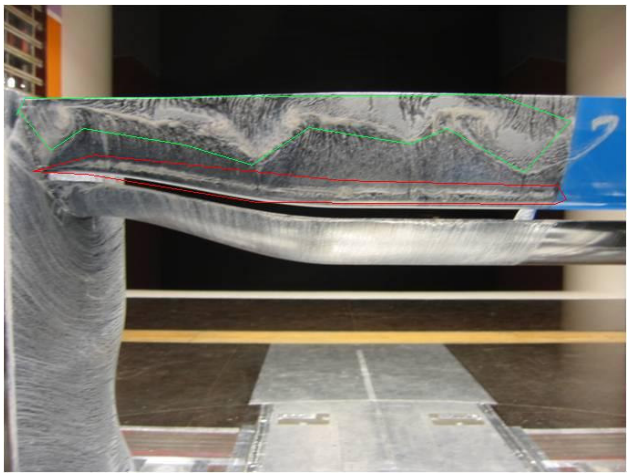

Figure 23. Oil streak flow visualization on the pressure surface of airfoil flap.

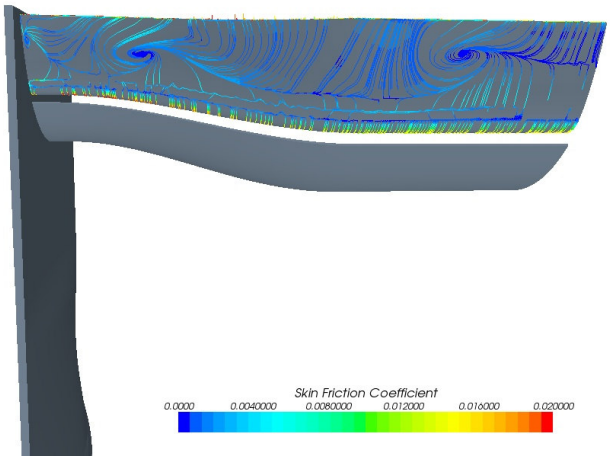

Figure 24. Streakline visualization colored by skin friction coefficient on pressure surface of airfoil flap.

VII. Conclusion

The γ-Re_θ transition model has been successfully implemented in STAR-CCM+, a commercial unstructured CFD code. After a process of calibration using published experimental data, the proprietary correlations omitted from publications by the originators of the model were synthesized. Sufficient information is included in this paper to guide others to perform a similar calibration. Using the synthesized correlations, the model was applied to several validation cases. The results of these validation cases compare favorably to the results shown by Langtry[5] for the same test cases.

During the course of this study, it was observed that the computational costs are significantly higher than fully turbulent calculations for two reasons. First, requirements on mesh resolution are greater (both wall-normal and streamwise spacing). Second, apart from the overhead of solving two additional transport equations, the interaction between the momentum, turbulence and transition equations requires more iterations for convergence. In addition, much more attention needs to be paid to the inflow or free-stream turbulence boundary conditions. Nevertheless, the successful application of the model to a realistic industrial flow simulation in this study, the Formula One multi-element rear wing, illustrates the value of the approach.

Appendix

The SST k-ω turbulence model,[11,12] as modified for use with the γ-Re$_\theta$ transition model[1-5], consists of two transport equations, for the turbulent kinetic energy, *k,* and the specific dissipation rate, ω,

$$\rho\frac{Dk}{Dt}=\frac{\partial}{\partial x_j}\left[\left(\mu+\sigma_k\mu_t\right)\frac{\partial k}{\partial x_j}\right]+\left(\gamma_{eff}\mu_t S^2-\rho k\frac{\partial u_j}{\partial x_j}\right)-\min\left[\max\left(\gamma_{eff},0.1\right),1\right]\rho\beta^*\omega k\,, \tag{3}$$

$$\rho\frac{D\omega}{Dt}=\frac{\partial}{\partial x_j}\left[\left(\mu+\sigma_\omega\mu_t\right)\frac{\partial \omega}{\partial x_j}\right]+\alpha\left(\mu_t S^2-\rho k\frac{\partial u_j}{\partial x_j}\right)-\rho\beta\omega^2+2\rho(1-F_1)\sigma_{\omega 2}\frac{1}{\omega}\frac{\delta k}{\delta x_j}\frac{\delta \omega}{\delta x_j}\,, \tag{4}$$

where *S* is the strain rate tensor modulus and γ_{eff} is the effective intermittency.

The turbulent viscosity is defined as:

$$\mu_t=\rho kT\,,\quad T=\min\left[\frac{1}{\max\left[\omega,SF_2/a_1\right]},\frac{0.6}{\sqrt{3}S}\right], \tag{5a, b}$$

where ρ is the density, u_j is the velocity vector, μ is the molecular viscosity, and μ_t is the eddy viscosity. The realizability constraint of Durbin[13] is reflected in the time scale (5a).

The functions F_1 and F_2 are given by:

$$F_1=\max\left[F_3,\tanh\left(\arg_1^4\right)\right],\quad arg_1=\max\left[\min\left(\frac{\sqrt{k}}{0.09\omega y},\frac{500\nu}{\omega y^2}\right),\frac{2k}{y^2CD_{k\omega}}\right],\quad CD_{k\omega}=\max\left(\frac{1}{\omega}\frac{\delta k}{\delta x_j}\frac{\delta \omega}{\delta x_j},\right), \tag{6a, b, c}$$

$$F_2=\tanh\left(\arg_2^2\right),\ arg_2=\max\left(\frac{2\sqrt{k}}{0.09\omega y},\frac{500\nu}{\omega y^2}\right), \tag{7a, b}$$

$$F_3=\exp\left(-(R_y/120)^8\right),\ \mathrm{R}_y=\rho y k^{1/2}/\mu\,, \tag{8a, b}$$

where *y* is the normal distance from the nearest wall.

The coefficients ϕ of the model are calculated from the blending function

$$\phi=F_1\phi_1+(1-F_1)\phi_2\,, \tag{9}$$

where the coefficients ϕ_1, ϕ_2 are:

$$\sigma_{k1}=0.85\,,\ \sigma_{\omega 1}=0.65\,,\ \beta_1=0.075\,,\ \alpha_1=\beta_1/\beta^*-\sigma_{\omega 1}\kappa^2/\sqrt{\beta^*}\,,$$

$$\sigma_{k2}=1.0,\ \sigma_{\omega 2}=0.856\,,\ \beta_2=0.0828\,,\ \alpha_2=\beta_2/\beta^*-\sigma_{\omega 2}\kappa^2/\sqrt{\beta^*}\,,$$

and $a_1 = 0.3$, $\kappa = 0.41$, $\beta^* = 0.09$.

A Neumann (zero-flux) wall boundary condition is specified for *k*, whereas $\omega = 6\nu/(\beta y^2)$ is specifically set in the wall-adjacent cells.

The γ-Re_θ transition model[1-5] consists of two transport equations: an equation for the intermittency, γ, and an equation for the transported transition momentum thickness Reynolds number, $\tilde{\mathrm{Re}}_{\theta t}$. These transport equations are written as

$$\rho\frac{D\gamma}{Dt}=\frac{\partial}{\partial x_j}\left[\left(\mu+\frac{\mu_t}{\sigma_\gamma}\right)\frac{\partial\gamma}{\partial x_j}\right]+F_{length}c_{a1}\rho S(\gamma F_{onset})^{0.5}(1-c_{e1}\gamma)+c_{a2}\rho\Omega\gamma F_{turb}(1-c_{e2}\gamma), \tag{10}$$

$$\rho\frac{D\tilde{\mathrm{Re}}_{\theta t}}{Dt}=\frac{\partial}{\partial x_j}\left[\sigma_{\theta t}(\mu+\mu_t)\frac{\partial\tilde{\mathrm{Re}}_{\theta t}}{\partial x_j}\right]+c_{\theta t}\frac{(\rho U)^2}{500\mu}(\mathrm{Re}_{\theta t}-\tilde{\mathrm{Re}}_{\theta t})(1-F_{\theta t}), \tag{11}$$

where Ω is the vorticity tensor modulus, and U is the local velocity magnitude. The parameters F_{length} and F_{onset} are used to control the length and onset location of transition respectively. F_{turb} and $F_{\theta t}$ are the parameters for controlling the destruction/relaminarization of the boundary layer and the boundary layer detector respectively.

The modeled transport equations are controlled by the following functions:

$$F_{onset}=\max(F_{onset2}-F_{onset3},0),\quad F_{turb}=\exp\left[-\left(R_T/4\right)^4\right], \tag{12a, b}$$

$$F_{onset2}=\min\left[\max(F_{onset1},F_{onset1}^4),2\right],\quad F_{onset1}=\frac{\mathrm{Re}_v}{2.193\mathrm{Re}_{\theta c}}, \tag{13a, b}$$

$$F_{onset3}=\max\left(1-\left(R_T/2.5\right)^3,0\right), \tag{14}$$

$$F_{\theta t}=\min\left\{\max\left[F_{wake}\cdot\exp\left[-\left(\frac{U^2}{375\Omega\nu\tilde{\mathrm{Re}}_{\theta t}}\right)^4\right],1-\left(\frac{c_{e2}\gamma-1}{c_{e2}-1}\right)^2\right],1\right\},\ F_{wake}=\exp\left[-\left(\frac{\mathrm{Re}_\omega}{10^5}\right)^2\right], \tag{15a, b}$$

$$\mathrm{Re}_v=\frac{\rho Sy^2}{\mu},\ \mathrm{R}_T=\frac{\rho k}{\mu\omega},\ \mathrm{Re}_\omega=\frac{\rho\omega y^2}{\mu}, \tag{16a, b, c}$$

where Re_v is the strain rate Reynolds number, R_T is a turbulent Reynolds number (commonly termed the viscosity ratio. $\mathrm{Re}_{\theta c}$ is the critical momentum thickness Reynolds number where the intermittency first appears in the boundary layer.

The model constants are c_{a1}=2.0, c_{e1}=1.0, c_{a2}=0.06, c_{e2}=50.0, c_α=0.5, σ_γ=1.0, $\sigma_{\theta t}$=2.0, $c_{\theta t}$=0.03.

Neumann (zero-flux) wall boundary conditions are applied for γ and $\tilde{\mathrm{Re}}_{\theta t}$. At inlets, γ=1.0 is applied and $\tilde{\mathrm{Re}}_{\theta t}$ is obtained from the freestream correlation for $\mathrm{Re}_{\theta t}$.

The effective intermittency, γ_{eff}, is obtained from

$$\gamma_{eff}=\max(\gamma,\gamma_{sep}), \tag{17}$$

$$\gamma_{sep}=\min\left[2\max\left(\frac{\mathrm{Re}_v}{3.235\mathrm{Re}_{\theta c}}-1,0\right)F_{reattach},2\right]F_{\theta t},\quad F_{reattach}=\exp\left(-\left(R_T/20\right)^4\right). \tag{18a, b}$$

To close the γ-Re_θ transition model, three correlations are required: for $\mathrm{Re}_{\theta t}$, $\mathrm{Re}_{\theta c}$ and F_{length}. Two correlations have been proposed for $\mathrm{Re}_{\theta t}$, the transition onset momentum thickness Reynolds number, defined in the free stream, based on a range of experimental data. The expression proposed Menter *et al.* [1] is:

$$\mathrm{Re}_{\theta t}=803.73\left(Tu+0.6067\right)^{-1.027}F_{\lambda,K}, \tag{19}$$

$$F_{\lambda,K}=\begin{cases}1-F_\lambda\cdot\mathrm{e}^{-Tu/3} & ;\lambda\le 0\\ 1+F_K\cdot\left(1-e^{-2Tu/3}\right)+0.556\left(1-e^{-23.9\lambda}\right)\cdot\mathrm{e}^{-Tu/3} & ;\lambda>0\end{cases} \tag{20}$$

$$F_\lambda=-10.32\lambda-89.47\lambda^2-265.51\lambda^3, \tag{21a}$$

$$F_K=0.0962\left(K\cdot10^6\right)+0.148\left(K\cdot10^6\right)^2+0.0141\left(K\cdot10^6\right)^3, \tag{22b}$$

$$\lambda_\theta = \frac{\theta^2}{\nu}\cdot\frac{dU}{ds},\ K = \frac{\nu}{U^2}\cdot\frac{dU}{ds},\ Tu = \frac{100(2k/3)^{1/2}}{U},\ \ \frac{dU}{ds} = \frac{\partial u_j}{\partial x_i}\frac{u_i u_j}{U^2}. \tag{23a, b, c, d}$$

The correlation of Eq. (19) was later modified by Langtry[5] to the following form:

$$\mathrm{Re}_{\theta t} = \begin{cases} \left[1173.51 - 589.428Tu + \dfrac{0.2196}{Tu^2}\right] F(\lambda, Tu); & Tu \le 1.3 \\ 331.5\left[Tu - 0.5658\right]^{-0.671} F(\lambda, Tu); & Tu > 1.3 \end{cases} \tag{24}$$

$$F(\lambda, Tu) = \begin{cases} 1 + e^{-(2Tu/3)^{1.5}} \cdot \left(12.986\lambda + 123.66\lambda^2 + 405.689\lambda^3\right) & ;\lambda \le 0 \\ 1 + 0.275\,\mathrm{e}^{-2Tu} \cdot \left(1 - \mathrm{e}^{(-35\lambda)}\right) & ;\lambda > 0 \end{cases} \tag{25}$$

Acknowledgments

The authors are grateful to Dr. Gary Ahlin of Computational Dynamics, London for providing the multi-element airfoil mesh and to Pointwise Inc. for the use of their Gridgen software used to create all the 2D meshes. Paul Malan thanks Professor Erik Dick of the University of Ghent and Professor Witold Elsner of Czetochowa University of Technology for useful and frank discussion during the initial stages of this work.

References

[1]Menter, F.R., Langtry, R.B., Likki, S.R., Suzen, Y.B., Huang, P.G., and Völker, S., "A Correlation-based Transition Model Using Local Variables Part 1 – Model Formulation," ASME GT2004-53452, *Proceedings of the ASME Turbo Expo*, *Power for Land Sea and Air*, June 14-17, 2004.

[2]Langtry, R.B., and Menter, F.R., "Transition Modeling for General CFD Applications in Aeronautics", *AIAA Paper 2005-522*, Reno, Nevada, 2005.

[3]Menter, F.R., Langtry, R.B., Völker, S.and Huang, P.G., "Transition Modelling for General Purpose CFD Codes," *ERCOFTAC Int. Symp. Engineering Turbulence Modelling and Measurements*, ETMM6, 2005.

[4]Menter, F.R., Langtry, R., and Volker, S., "Transition Modelling for General Purpose CFD Codes," *Flow, Turbulence and Combusion,* Vol. 77, pp.277-303, 2006.

[5]Langtry, R.B., "A Correlation-based Transition Model Using Local Variables for Unstructured Parallelized CFD Codes," Dr.-Ing thesis, Institute of Thermal Turbomachinery and Machinery Laboratory, University of Stuttgart, 2006.

[6]Piotrowski., W., Elsner, W. and Drobniak, S., "Transition Prediction on Turbine Blade Profile with Intermittency Transport Equation," ASME GT2008-50796, *Proceedings of the ASME Turbo Expo, Power for Land Sea and Air*, June 9-13, 2008.

[7]Suluksna, K., Dechaumphai, P. and Juntasaro E., "Correlations for Modeling Transitional Boundary Layers under Influences of Freestream Turbulence and Pressure Gradient*," Int. J. Heat and Fluid Flow* (to be published).

[8]STAR-CCM+ Software Package, Version 3.06, CD-adapco, Melville NY (to be released).

[9]Demirdzic, I. and Muzaferija, S., "Numerical Method for Coupled Fluid Flow, Heat Transfer and Stress Analysis Using Unstructured Moving Meshes with Cells of Arbitrary Topology," *Comput. Methods Appl. Mech. Engrg*., 1995.

[10]Weiss, J.M. and Smith, W.A., "Preconditioning Applied to Variable and Constant Density Flows," *AIAA Journal*, Vol. 33, No. 11, 1995, pp. 2050-2057.

[11]Menter, F. R., "Two-Equation Eddy Viscosity Models for Engineering Applications," *AIAA Journal*, Vol. 32, No. 8, 1994, pp. 1598-1605.

[12]Vieser, W., Thomas Esch, T. and Menter, F., "Heat Transfer Predictions using Advanced Two-Equation Turbulence Models, " *CFX Technical Memorandum* CFX-VAL10/0602, ANSYS Inc., 2002.

[13]Durbin, P., "On the *k*-ε Stagnation Point Anomaly," *International Journal of Heat and Fluid Flow*, Vol. 17, pp. 89-90, 1995.

[14]ERCOFTAC (European Research Community on Flow, Turbulence, Combustion) Nexus. [online database], URL: http://ercoftac.mech.surrey.ac.uk/ [cited 15 Feb 2008].

[15]Schubauer, G.B. and Klebanoff, P.S. "Contributions on the Mechanics of Boundary Layer Transition," *NACA Technical Note 3489*, 1955.

[16]Chaput, E., "Chapter III: Application-Oriented Synthesis of Work Presented in Chapter II," *Notes on Numerical Fluid Mechanics*, Vol. 58, Vieweg Braunschweig, Wiesbaden, pp. 327-346, 1997.

[17]Zierke, W.C. and Deutsch, S., "The Measurement of Boundary Layers on a Compressor Blade in Cascade, Vol. 1 --- Experimental Technique, Analysis and Results," *NASA CR 185118*, 1989.

[18]Ubaldi, M., Zunino, P., Campora, U. and Ghiglione, A., "Detailed Velocity and Turbulence Measurements of the Profile Boundary Layer in a Large Scale Turbine Cascade," *Proceedings of the International Gas Turbine and Aeroengine Congress and Exhibition*, Birmingham, UK, ASME 96-GT-42, 1996.